JACS
JOURNAL OF THE AMERICAN CHEMICAL SOCIETY
Article
pubs.acs.org/JACS

Molecular Photoconductor with Simultaneously Photocontrollable Localized Spins

Toshio Naito,*[,†] Tomoaki Karasudani,[†] Shigeki Mori,[†] Keishi Ohara,[†] Kensuke Konishi,[†] Takahiro Takano,[‡] Yukihiro Takahashi,[‡,∥] Tamotsu Inabe,[‡,∥] Sadafumi Nishihara,[⊥] and Katsuya Inoue[⊥]

[†]Graduate School of Science and Engineering, Ehime University, Matsuyama 790-8577, Japan

[‡]Graduate School of Science and [∥]Graduate School of Chemical Sciences and Engineering, Hokkaido University, Sapporo 060-0810, Japan

[⊥]Department of Chemistry, Graduate School of Science, Hiroshima University, Higashi-Hiroshima 739-8526, Japan

Supporting Information

ABSTRACT: UV irradiation reversibly switches a new insulating and nonmagnetic molecular crystal, BPY[Ni(dmit)$_2$]$_2$ (BPY = *N*,*N*′-ethylene-2,2′-bipyridinium; Ni(dmit)$_2$ = bis(1,3-dithiole-2-thione-4,5-dithiolato)nickelate(III)), into a magnetic conductor. This is possible because the bipyridyl derivative cations (BPY^{2+}) trigger a photochemical redox reaction in the crystal to produce a change of ∼10% in the filling of the Ni(dmit)$_2$ valence band, leaving localized spins on the BPY themselves. In the dark, almost all of the BPY molecules are closed-shell cations, and most of the Ni(dmit)$_2$ radical anions form spin-singlet pairs; thus, this material is a diamagnetic semiconductor. Under UV irradiation, a photocurrent is observed, which enhances the conductivity by 1 order of magnitude. Electron spin resonance measurements indicate that the UV irradiation reversibly generates carriers and localized spins on the Ni(dmit)$_2$ and the BPY, respectively. This high photoconductivity can be explained by charge transfer (CT) transitions between Ni(dmit)$_2$ and BPY in the UV region. In other words, the photoconduction and "photomagnetism" can be described as reversible optical control of the electronic states between an ionic salt (BPY^{2+}/[Ni(dmit)$_2$]$^-$, nonmagnetic insulator) and a CT complex (BPY$^{2(1-\delta)+}$/[Ni(dmit)$_2$]$^{(1-\delta)-}$ ($\delta \approx 0.1$), magnetic conductor) in the solid state.

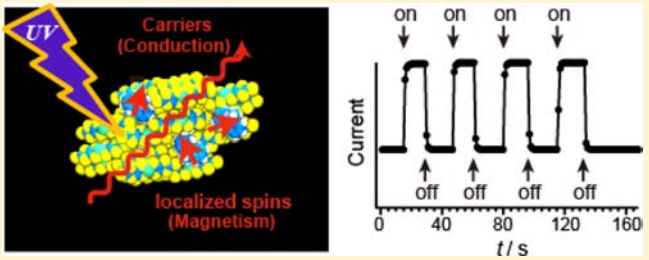

INTRODUCTION

Crystalline molecular charge transfer (CT) complexes exhibit various metastable states. Optical or phase transitions between these states might serve as switches if the transitions involve qualitative and reversible changes in the conduction, magnetic, and/or optical properties.[1] Recently, there has been great interest in the physical properties of the complexes immediately after photoexcitation (PE), especially photoinduced phase transitions (PIPT).[2−10] The examination of the PE of molecular CT complexes seems to be leading to the discovery of new phenomena applicable to emerging technologies. For example, time-resolved spectroscopy has revealed that an organic salt, (EDO-TTF)$_2$PF$_6$ (Chart1), exhibits a metal-to-insulator transition within 20 fs at room temperature by PE.[2,3] Furthermore, the switching behavior of α-(ET)$_2$I$_3$[4−8] has been applied not only to a thyristor[7] but also to nonlinear optics.[9,10]

The charge degree of freedom is particularly large in molecular CT complexes, which often produces the metastable states.[11−16] In some compounds, alternately π-stacked electron donor and acceptor molecules can be transformed from neutral to ionic by the control of temperature and hydrostatic pressure. Such a neutral-ionic (NI) phase transition often leads to ferroelectricity.[17] The NI transition has also been attracting interest from a PIPT perspective for more than 10 years.[18,19] Spin-crossover (SCO) metal-complex compounds exhibiting conversion between high-spin (HS) and low-spin (LS) states are known to be phase-transition compounds for magnetic materials, and the photoinduced LS→HS transition of SCO compounds is known as light-induced excited spin-state trapping.[20,21] Related work in this area is rapidly advancing.[22−25]

Aside from studies concerning PE, there is another large group of molecular CT complexes which have been attracting global interest for a long time. They are magnetic conductors having both carriers and localized spins. For example, by selecting R^1,R^2 in Cu(R^1,R^2-DCNQI)$_2$ (2,5-disubstituted *N*,*N*′-dicyanoquinonediimine; R^1,R^2 = alkyl groups, halogen atoms, etc.; Chart 1),[26−31] they exhibit behavior like a heavy fermion system with weak ferromagnetism[32−40] and re-entrant metal−insulator (MI) transitions.[41−44] Some CT complexes of bis(ethylenedithio)tetraselenafulvalene (BETS)[45−47] exhibit both magnetic ordering and superconductivity,[48−50] while some BETS complexes exhibit "magnetic-field-induced super-

Received: June 27, 2012
Published: September 4, 2012

   dx.doi.org/10.1021/ja306260b | *J. Am. Chem. Soc.* 2012, 134, 18656−18666

Chart 1. Component Molecules for Conductors

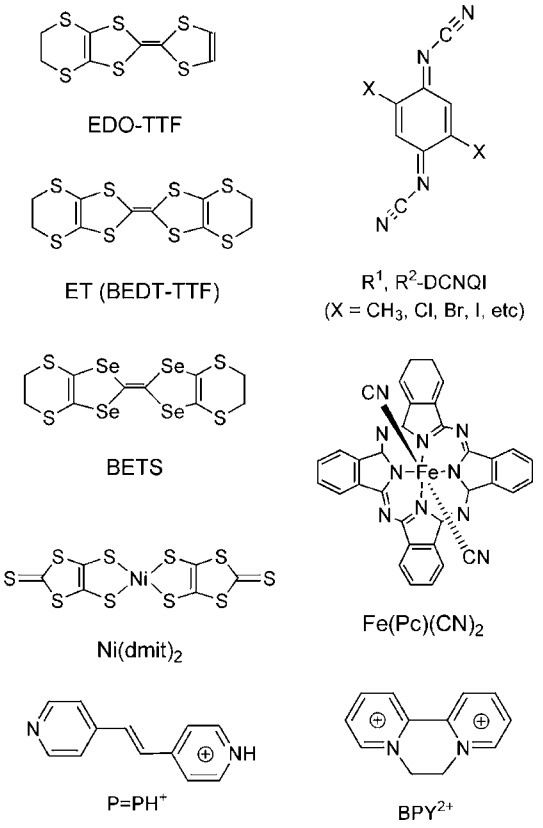

conductivity".[50,51] All of these BETS complexes are in sharp contrast with conventional superconductors, since a magnetic field usually suppresses the occurrence of superconductivity. Magnetic fields generally increase electrical resistivity of materials. However, a CT complex of the iron(III) phthalocyanine derivative $Fe(Pc)(CN)_2$ loses a substantial portion (up to 99.8%) of its original resistivity under pressure and an applied magnetic field, which is denoted "giant negative magnetoresistance" (GNR).[52−57] GNR is often observed in many Perovskites and the mechanism has been studied.[58−60] All of these unusual responses to magnetic fields originate from the interaction between carriers and localized spins.

There could still be an undiscovered compound containing all of the attributes above: a molecular CT complex having both carriers and localized spins in the photoexcited state (a "photo-magnetic-conductor"). Despite the extensive prior studies, to the authors' knowledge, there have been no reports of such materials. There are preceding studies for realizing a magnetic metal system at the ground states by utilizing magnetic metal complex or stable free radical organic molecules as the counter cations of the bis(1,3-dithiole-2-thione-4,5-dithiolato)nickelate-(III) ($Ni(dmit)_2$) radical anion complexes.[61−64] Such magnetic molecules have localized spins at their ground states, yet they are generally bulky, which causes the following two problems: (1) It is difficult to make the spins interact with neighboring molecules through their ligands/protecting groups; the magnetic interaction is usually indirect and often too weak to affect the behavior of carriers in a qualitative manner. (2) The conduction pathways comprised of the $Ni(dmit)_2$ molecules are interrupted by the bulky magnetic molecules, which make the resultant CT complexes insulators at the ground states. Accordingly, they frequently turned out unsuitable for interaction with carriers on planar π-conjugated molecules like $Ni(dmit)_2$. In the meantime, if we utilize another kind of planar π-conjugated molecule also for localized spins, the interaction between the carriers and localized spins will be too strong and will result in diamagnetic/antiferromagnetic insulators, i.e., practically nonmagnetic insulators, at their ground states. However, if we irradiate such CT complexes to excite and produce carriers and localized spins, this problem will be solved. Here, we must select planar π-conjugated molecules of a similar size to or slightly smaller than the $Ni(dmit)_2$ molecule for assuring both of conduction pathways and strong interaction by maximum overlap of the two kinds of molecules having similar energy levels and molecular orbital symmetries. Additionally, the cations are desired to be 2+ for the following reasons: (1) enhancement of the volume ratio of the $[Ni(dmit)_2]$ monoanions in the unit cell, which will lead to their closer packing; (2) at the same time, lower volume ratio of the cations will lead to isolation of the cations from each other, being advantageous for accommodation of localized spins when they are photoexcited; (3) minimizing the amplitudes of periodic potential against the carriers movement; the larger the charge of the cations become, the more often the carriers are trapped. In this way, the planar π-conjugated molecules can provide either of localized spins or carriers depending on the counterparts we select; the bulky localized spin sources do not have such flexibility. By analogy to photochemical redox reactions, it was anticipated that a larger number of electrons should be transferred in a CT transition in photochemical redox pairs than in other donor−acceptor pairs. For example, the $Ni(dmit)_2$ complexes with bipyridine derivative dications belong to the promising candidates, since many bipyridine derivatives are known to be redox-reactive under irradiation.[65−67] Based on this idea, a series of molecular CT complexes containing photoinduced redox-active species were examined, and a new molecular crystalline material, $BPY[Ni(dmit)_2]_2$ (BPY = *N*,*N*′-ethylene 2,2′-bipyridinium), was found to be a "photo-magnetic-conductor". Herein we report its synthesis, structure, and physical properties, both in the dark and upon UV irradiation.

RESULTS AND DISCUSSION

Crystal Structure and Molecular Charges in the Dark.

As the structure is complicated, the molecular arrangement of $Ni(dmit)_2$ and that of BPY will be discussed separately. The former forms the conduction pathways in $BPY[Ni(dmit)_2]_2$ (Figure 1). The asymmetric unit of the crystal includes two $Ni(dmit)_2$ molecules with a dihedral angle of ∼50°. Although they are crystallographically independent, the two $Ni(dmit)_2$ molecules have nearly identical structures, suggesting an equal charge distribution between them. In addition, the bond lengths indicate that both of the crystallographically independent two $Ni(dmit)_2$ molecules should be monoradical anions $[Ni(dmit)_2]^-$.[68] This is consistent with the fact that BPY carries a charge of 2+, based on the spectra of $BPY{\cdot}Br_2$ in solution and $BPY[Ni(dmit)_2]_2$ in the solid state (Figure 2 and Figure S2 in the Supporting Information). Therefore, hereafter their electronic states in the dark are denoted $[Ni(dmit)_2]^-$ and BPY^{2+}. There are many S−S interatomic distances shorter than twice the van der Waals radius (<3.70 Å; denoted "short contacts" below) among the $Ni(dmit)_2$ molecules. The crystal structure consists of various types of $Ni(dmit)_2$ columns running in different directions, crossing each other, interconnected by the S−S short contacts. Therefore, the whole

dx.doi.org/10.1021/ja306260b | J. Am. Chem. Soc. 2012, 134, 18656−18666

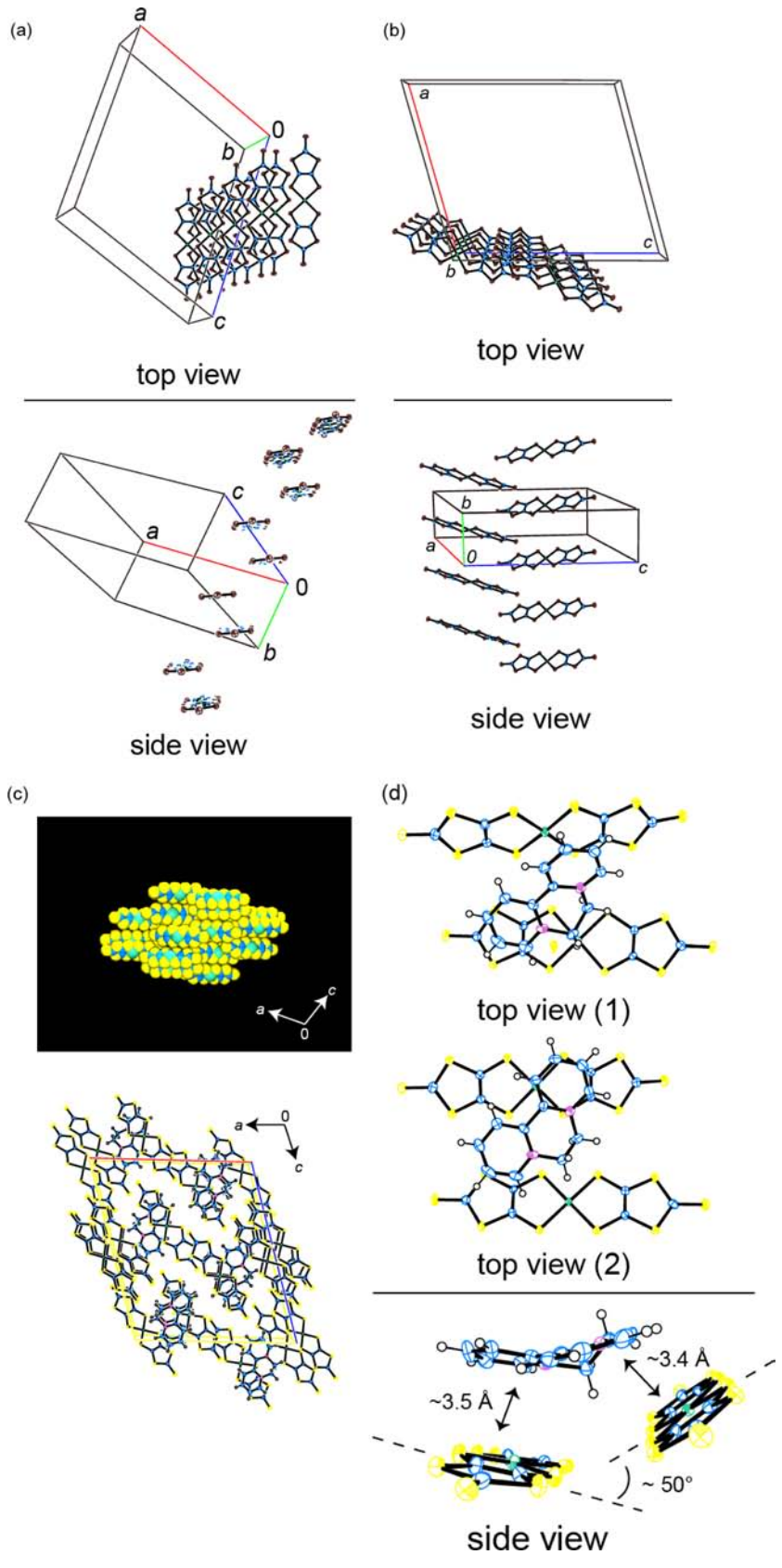

Figure 1. (a,b) Relation between neighboring molecular columns of $Ni(dmit)_2$: (a) and (b) depict different pairs of columns from each other. (c) (upper) Molecular packing of $Ni(dmit)_2$ in the *ac*-plane, and (lower) molecular packing of $Ni(dmit)_2$ and BPY in the *ac*-plane. (d) Close-up view of relative molecular arrangement around $Ni(dmit)_2$ and BPY.

dx.doi.org/10.1021/ja306260b | J. Am. Chem. Soc. 2012, 134, 18656−18666

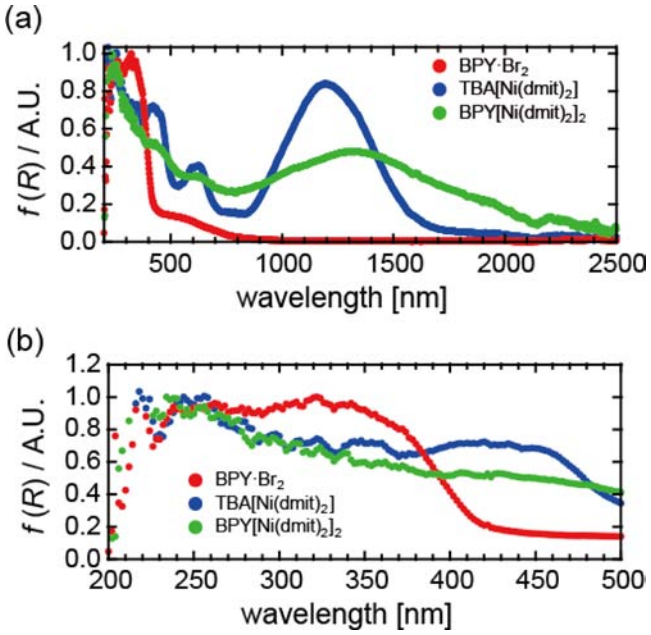

Figure 2. Diffuse reflectance spectra of TBA[Ni(dmit)$_2$] and BPY·Br$_2$ dispersed in KBr, where TBA = n-$(C_4H_9)_4N$: (a) whole spectra and (b) close-up view.

Ni(dmit)$_2$ molecular arrangement can be better described as a three-dimensional close-packed network of Ni(dmit)$_2$ (Figure 1c), instead of a columnar structure. This type of mixed-stacking structure is advantageous for interaction between [Ni(dmit)$_2$]$^-$ and BPY^{2+}.

There is one crystallographically independent BPY molecule in the asymmetric unit. The BPY molecules are inserted into small spaces in the network, surrounded by Ni(dmit)$_2$. The bond lengths of the BPY cations are normal in comparison with its parent molecule 2,2′-bipyridyl, which is usually completely planar.[69,70] However in this salt, interestingly, the molecular plane of the bipyridyl skeleton is distorted in such a way so that each pyridine ring is nearly parallel to either of the two crystallographically independent Ni(dmit)$_2$ molecules (Figure 1d). The distortion is partly because of the geometrical requirement of the bridging ethylene group. It will destabilize BPY, will enhance the reactivity, and will favor the CT interaction with surrounding chemical species more than 2,2′-bipyridyl.[71] The interplanar distances between the pyridine rings and Ni(dmit)$_2$ are ∼3.4 and ∼3.5 Å, both of which suggest $\pi-\pi$ interactions.

Cation−Anion Interaction. Figure 3a and Table S1 in the Supporting Information show the overlap and the transfer integrals of the intermolecular interactions in this material, as calculated using an extended Hückel method. The parameters of the calculation are listed in Table S2. The Ni(dmit)$_2$ (LUMO)−Ni(dmit)$_2$ (LUMO) interaction is important primarily for electrical conduction, while the remainder of the interactions are important primarily for the relationship between the cations (localized spins) and anions (carriers). Among the interactions associated with conduction (S_3, S_5, S_8, S_9, S_{11}, S_{13} and S_{14}), S_3 is dominant. The remaining interactions are in various directions with different strengths, averaging out in a rather small anisotropy. These interactions realize the three-dimensional network of conduction pathways.

Among the BPY−Ni(dmit)$_2$ interactions (S_2, S_4, S_6, S_7, and S_{10}), only S_{10} is significantly large, while S_2, S_6 and S_7 are the next largest, comparable to or larger than most of the Ni(dmit)$_2$−Ni(dmit)$_2$ interactions (S_5, S_9, S_{11}, S_{13}, and S_{14}). Assuming that the crystal structure remains unchanged under UV irradiation, the result of this calculation is that there could be significant interaction between BPY^{2+} and [Ni(dmit)$_2$]$^-$ both in the dark and UV irradiated conditions.

In fact, the UV−vis and NIR spectra of BPY[Ni(dmit)$_2$]$_2$ contain much broader and slightly shifted peaks compared to those of BPY·Br$_2$ and [n-$(C_4H_9)_4N$][Ni(dmit)$_2$] (Figures 2 and S2). Figure S2c clearly indicates that the isolated [Ni(dmit)$_2$]$^-$ does not absorb the light with λ < 500 nm, which means the absorption peaks in the UV region are from (i) local excitation of BPY, (ii) CT between anions, or (iii) CT between anions and cations. In particular, the line shape at 330−500 nm of BPY[Ni(dmit)$_2$]$_2$ is clearly different from that of either BPY·Br$_2$ or [n-$(C_4H_9)_4N$][Ni(dmit)$_2$]. This is consistent with the assignment of the overlapped broad peaks (∼250−800 nm) to a series of CT transitions between BPY^{2+} and [Ni(dmit)$_2$]$^-$, which is also supported by the calculated band structure (see below). These facts indicate that there should be interaction between BPY^{2+} and [Ni(dmit)$_2$]$^-$ in BPY[Ni(dmit)$_2$]$_2$. Here, the highest occupied molecular orbital (HOMO) and the lowest unoccupied molecular orbital (LUMO) should be based on the neutral-molecule states. On the basis of the band calculation (in the next section) and the solution spectra calculated using Gaussian09 (Figure S2c,d),[72,73] the peak at ∼900−1600 nm in the [n-$(C_4H_9)_4N$][Ni(dmit)$_2$] spectra corresponds primarily to the HOMO→LUMO transition of Ni(dmit)$_2$, while most of the peaks of BPY (∼220 and ∼280−330 nm) correspond to the (HOMO−n)→HOMO (n = 1−4) transitions. Thus, in the photoexcited state, the majority of the unpaired electrons are accommodated in the LUMO of Ni(dmit)$_2$ and in the HOMO of BPY, respectively. These orbitals are well overlapped based on the calculation, which signifies a strong interaction between them.

Here a brief comment should be made on the crystal structure under UV irradiation. We carried out a single-crystal X-ray structural analysis with irradiating the crystal with UV, which gave an identical result with the crystal structure without UV irradiation. There may be some different reasons for this; for example, the UV light did not penetrate deeply enough into the sample to bring about a structural change in a substantial part of the crystal. Accordingly, thus far we have not obtained any experimental evidence for or against a crystal structural change under UV irradiation. Some different methods will be required to elucidate whether a structural change should happen or not in the photoexcited state.

Band Structure in the Dark. Figure 3b shows the calculated band structure within the framework of an extended Hückel tight-binding band approximation.[74] Because of the molecular close packing of Ni(dmit)$_2$, the bands around the Fermi level E_F (∼−10.59 eV; Figure 3c), which originate primarily from the LUMO of Ni(dmit)$_2$, are warped in a rather isotropic way. In addition, the molecular orbitals of BPY and Ni(dmit)$_2$ mix to form energy bands. Accordingly, many of the interband transitions in the UV region correspond to the CT bands between BPY^{2+} and [Ni(dmit)$_2$]$^-$ (Figure 3d). The amount of charge (δ) transferred in the CT transition is

$$\delta = \frac{|\alpha^2 - \beta^2|}{\alpha^2 + \beta^2} f \qquad (1)$$

dx.doi.org/10.1021/ja306260b | J. Am. Chem. Soc. 2012, 134, 18656−18666

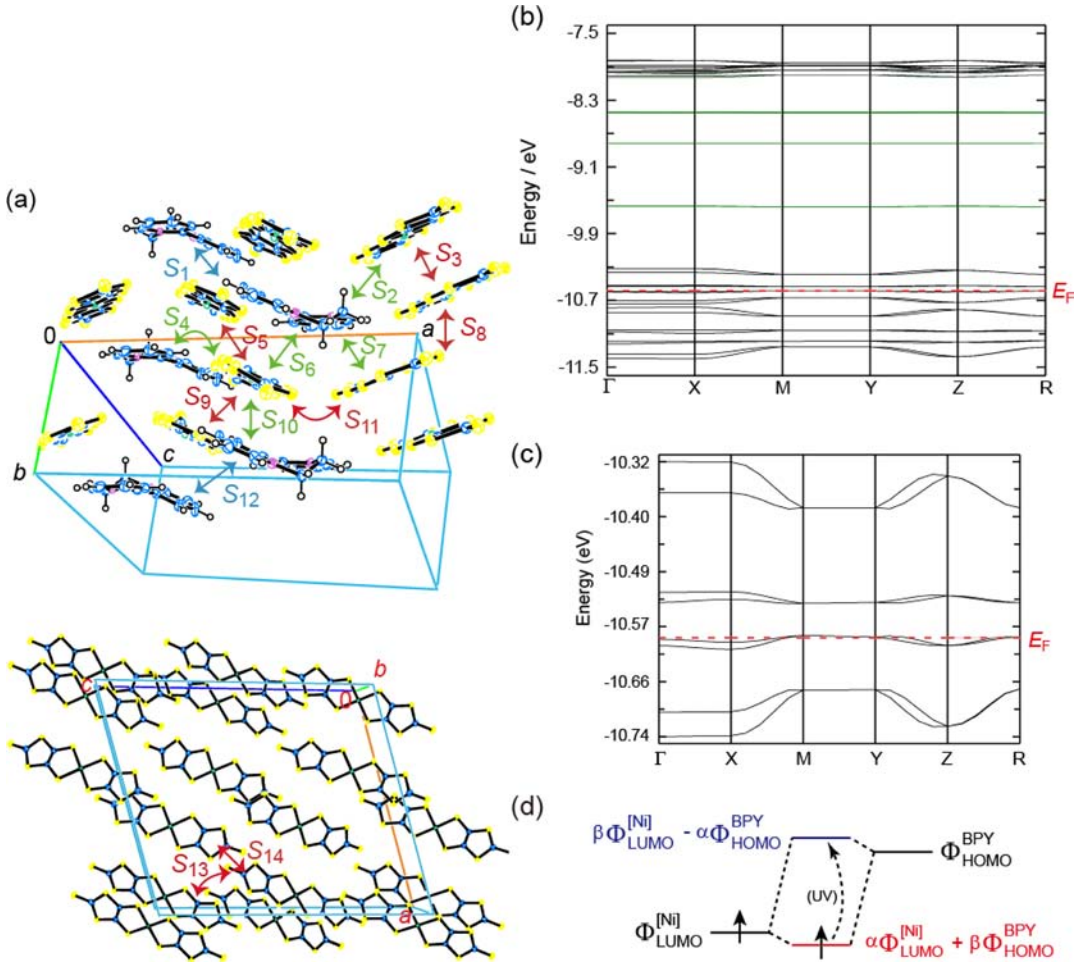

Figure 3. (a) Selected pairs for calculation of overlap integrals S_j (j = 1−14) involving Ni(dmit)$_2$ and BPY. For simplicity, interactions between anions are shown in Figure S1 in the Supporting Information. (b) Extended Hückel tight-binding band structure considering BPY and Ni(dmit)$_2$ both. Green/black curves denote the bands primarily originated from BPY/Ni(dmit)$_2$. Red broken line marked with E_F denotes Fermi level. Γ, X, M, Y, Z, R correspond to (0,0,0), (0.5,0,0), (0.5,0.5,0), (0,0.5,0), (0,0,0.5), (0.5,0.5,0.5) in reciprocal space, respectively. (c) Close-up view of band structure around E_F. (d) Schematic description of CT transition between Ni(dmit)$_2$ (abbreviated as [Ni]) and BPY.

where α and β are the coefficients in Figure 3d, and f is the oscillator strength. The series of broad bands in the UV−vis−NIR region observed for BPY[Ni(dmit)$_2$]$_2$ (Figure 2) can be qualitatively understood as an envelope of various CT bands, as stated in the previous section.

There is an additional important feature in the band structure: the bands are rather narrow, as is often the case in solid state Ni(dmit)$_2$. In particular, the narrow band at E_F has two opposing effects. Strong electron correlation tends to open a band gap at E_F, while the slightest change in the formal charge of the Ni(dmit)$_2$ anions produces a large Fermi surface, i.e., a stable metallic band structure. In fact, BPY[Ni(dmit)$_2$]$_2$ actually exhibits semiconducting behavior with a small band gap, in spite of the calculated metallic band structure. This is considered to be an effect of the strong electron correlation, which was not considered in the band structure calculation. As the small bandwidth at E_F has yet to realize the other effect, it is intriguing to enforce the CT between Ni(dmit)$_2$ and BPY beyond the restrictions of thermodynamic equilibrium, which is possible with light.

Conduction Properties. As shown in Figure 4 BPY[Ni(dmit)$_2$]$_2$ exhibits semiconducting behavior with an activation energy of E_a = 0.11 eV (~1400 K) and a dark resistivity of ρ_{RT} = 63 Ω·cm (RT = room temperature; surface resistivity R_{sq} = 1.2 × 10^5 Ω) at 300 K. Considering the diamagnetism (see below) and the activation energy being much larger than RT, the observed ρ_{RT} is unusually low.

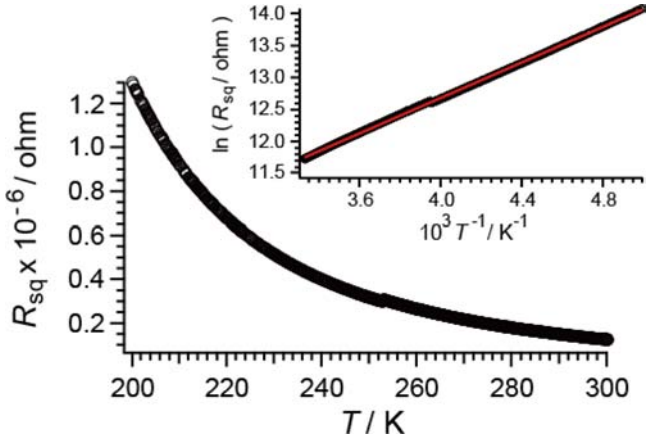

Figure 4. Temperature dependence of electrical resistivity of single crystals of BPY[Ni(dmit)$_2$]$_2$ under the dark condition measured with current along [010] using a four-probe method. Inset shows the Arrhenius plot of the same data. Red line is the best-fit line, giving the activation energy of 0.11 eV.

dx.doi.org/10.1021/ja306260b | J. Am. Chem. Soc. 2012, 134, 18656−18666

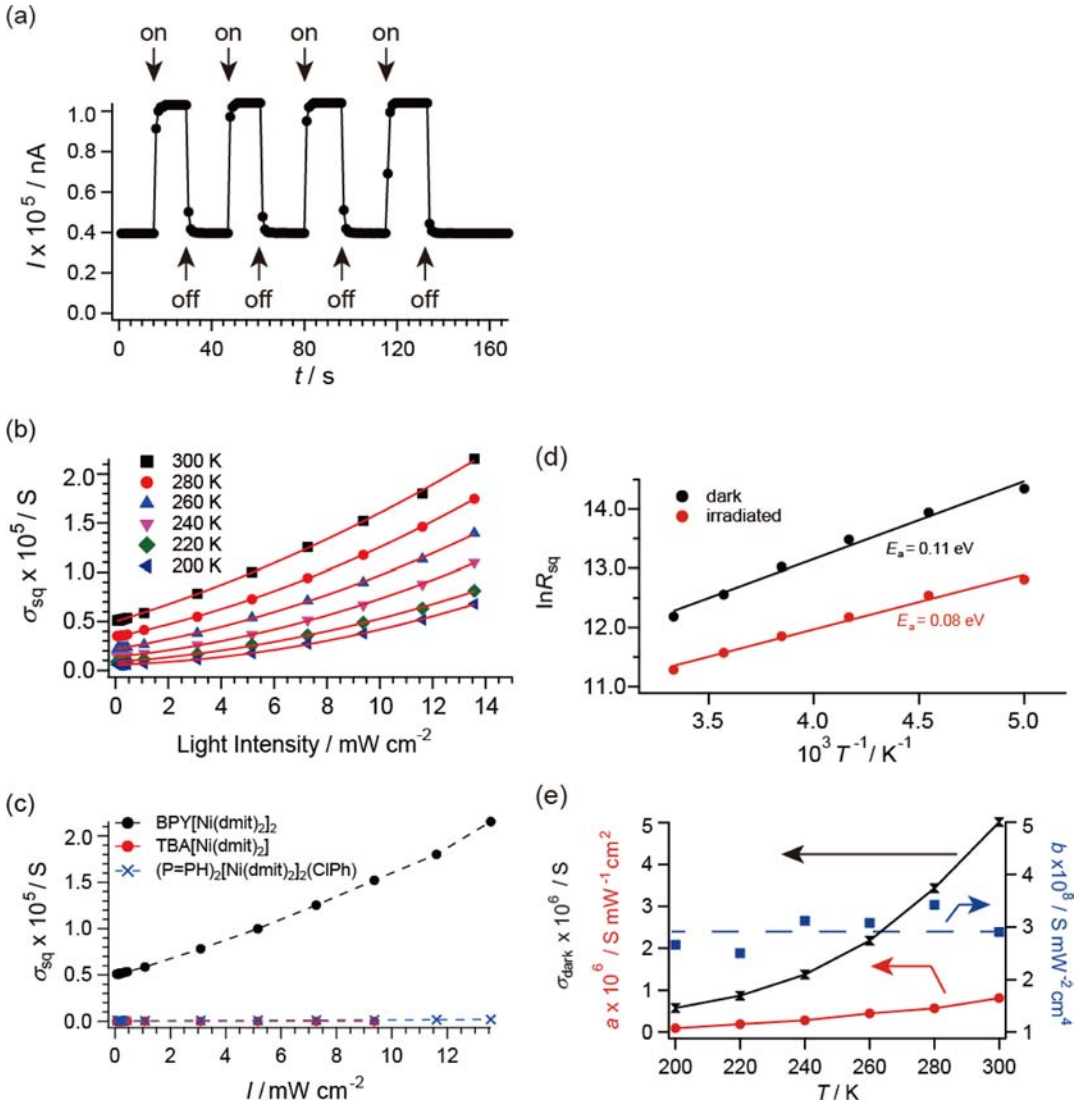

Figure 5. Photoconduction of single crystals of BPY[Ni(dmit)$_2$]$_2$ measured with current along [010] using a two-probe method in vacuo. (a) Photoconductive response to UV (375 nm) at 300 K (applied voltage = 0.1 V, light intensity = 11.6 mW cm^{-2}). (b) Dependence of photoconductivity σ_{ph} on light intensity and temperature, shown as surface conductivity σ_{sq}. Red curves in (b) are fitting curves using eq 2 and parameters in Table S4. (c) Comparison of surface conductivity under UV irradiation σ_{sq} between [*n*-(C$_4$H$_9$)$_4$N][Ni(dmit)$_2$], (P═PH)$_2$[Ni(dmit)$_2$]$_2$(ClPh)[83] and BPY[Ni(dmit)$_2$]$_2$ (ClPh = C$_6$H$_5$Cl, TBA = *n*-(C$_4$H$_9$)$_4$N). For P═PH, see Chart1. (d) Activation energies of conduction with/without UV irradiation. R_{sq} means surface resistivity. (e) Contribution of photoconductivity (temperature dependence of σ_{dark} (black), *a* (red) and *b* (blue) in eq 2).

The BPY salt exhibits the most evident response in its electron spin resonance (ESR) and conduction properties when it is irradiated with a UV light source (~250−450 nm), while it exhibits only a slight response to light of other wavelengths. This is unique, because known photoconductors do not exhibit wavelength selectivity so long as their energies exceed the threshold required for carrier generation. In this salt, the threshold (energy gap for conduction) is ~5000 nm, as estimated from the E_a (0.11 eV) in the dark. The UV region covers the CT transitions between BPY^{2+} and [Ni(dmit)$_2$]$^-$.

Figure 5a shows the photocurrent *I* response to UV irradiation (375 nm; 3.3 eV) at RT. A rapid, clear, and stable response is observed. This material is stable against UV irradiation: even after continuous exposure to UV in air at RT for 1−2 h, the ESR spectra and the X-ray oscillation photographs are no different from those before the exposure.

The BPY salt photoconductivity σ_{ph} was examined under UV irradiation (375 nm) with varying temperature and light intensity (Figure 5b and Table S3). BPY[Ni(dmit)$_2$]$_2$ exhibits higher dark conductivity than many other [Ni(dmit)$_2$]$^-$ compounds with closed-shell organic cations by ~10^3 times or more.[75] Considering the high σ_{dark}, the $\sigma_{ph}/\sigma_{dark}$ ratio is rather high in this material (>10 at 200 K). For comparison, [*n*-(C$_4$H$_9$)$_4$N][Ni(dmit)$_2$] exhibits hardly any photoconductivity ($\sigma_{ph}/\sigma_{dark} \leq 2$) (Figure 5c), though it also has many conduction pathways based on the S−S short contacts among the [Ni(dmit)$_2$]$^-$.

Under UV irradiation, BPY[Ni(dmit)$_2$]$_2$ exhibits semiconducting behavior with a smaller activation energy (0.08 eV) than it does in the dark (0.11 eV) (Figure 5d).

It is interesting that the conductivity is enhanced with the light intensity in a nonlinear way. Usually, photoconductivity increases with light intensity linearly, because the number of

dx.doi.org/10.1021/ja306260b | J. Am. Chem. Soc. 2012, 134, 18656−18666

photoexcited carriers should be proportional to the number of photons absorbed. As shown in Figure 5b, the observed behavior is well reproduced by a polynomial (eq 2; for the parameters obtained, see Table S4),

$$\sigma_{sq} = \sigma_{dark} + aI + bI^2 \quad (2)$$

where σ_{dark}, a, and b are fitting parameters, and I is the light intensity. The data are not reproduced with any other fitting function including exponential and/or higher polynomial terms. This result can be explained as follows. The observed photoconduction is actually the sum of three different contributions: dark conductivity, photoconductivity with the standard mechanism mentioned above ("standard photoconduction"), and a third term (Figure 5e). The temperature dependence of the first term (σ_{dark}) obtained from the curve-fitting analysis gives an activation energy of 0.11 eV, which agrees with the directly measured value (Figure 4; 0.11 eV), consistent with its physical meaning. The second term (aI) in eq 2 describes the contribution of the standard photoconduction. The third term (bI^2) in eq 2 describes a genuine photoinduced conduction, because the temperature dependence of b (i.e., activation energy ~0) is qualitatively different from the dark behavior (σ_{dark}), and thus thermally inaccessible to the dark state. The third parameter (b) is characteristic in that it is nearly temperature independent, unlike the other contributions, which is suggestive that its dominant origin is independent of temperature. The I^2 dependence of the third term is suggestive of the importance of a cooperative effect.[23,76] One such origin is considered to be the electron−electron and/or spin−spin interaction among the photoexcited carriers and/or photoexcited localized spins. Considering the temperature dependence, the third term (bI^2) should indicate metallic (photo)conduction. Like BPY[Ni(dmit)$_2$]$_2$, metals with small band widths and localized spins can exhibit nearly temperature-independent conduction because of the strong electron−electron and/or spin−spin interactions. This interpretation is consistent with the magnetic properties under UV irradiation discussed below, and also with a theoretical study on PIPT of ionic-to-neutral transitions based on a one-dimensional extended Peierls−Hubbard model.[77] Although BPY[Ni(dmit)$_2$]$_2$ is not a one-dimensional system, there are many important similarities shared between BPY[Ni(dmit)$_2$]$_2$ and the model system in the theoretical study: a mixed-stack organic charge-transfer complex, the importance of three-dimensional interactions (cooperative effect), the character of the phase transition (ionic-to-neutral), the nonlinear dependence on the light intensity, and the effectiveness of off-resonant irradiation. In fact, the key feature of such a system, i.e., the nonlinear dependence, has been widely observed in many cases of PIPT with respect to the magnetic, conduction, and optical properties.[78] The relative intensities of the three different contributions (σ_{dark}, aI, and bI^2) obtained here are not intrinsic and depend on the experimental conditions such as light intensities and wavelengths, incident angles, sample thickness, etc. However, in addition to the wavelength selectivity, the finding of this nonlinear light intensity-dependence indicates that the mechanism of this photoconductivity should be different from the known mechanism common to many other photoconductors.

Magnetic Properties. BPY[Ni(dmit)$_2$]$_2$ exhibits a diamagnetic susceptibility $\chi = -(9 \pm 1) \times 10^{-4}$ emu mol^{-1} in the dark (Figure 6). Because each [Ni(dmit)$_2$]$^-$ (= radical monoanion) should possess $S = {}^1/_2$ spins, the observed susceptibility indicates strong antiferromagnetic interactions among the [Ni(dmit)$_2$]$^-$ species, which makes the material diamagnetic (spin-singlet) at the ground state. This antiferromagenic interaction is consistent with the calculated overlap integrals, among which S_3 is dominant and positive, corresponding to a strong antiferromagnetic interaction between the [Ni(dmit)$_2$]$^-$ species.

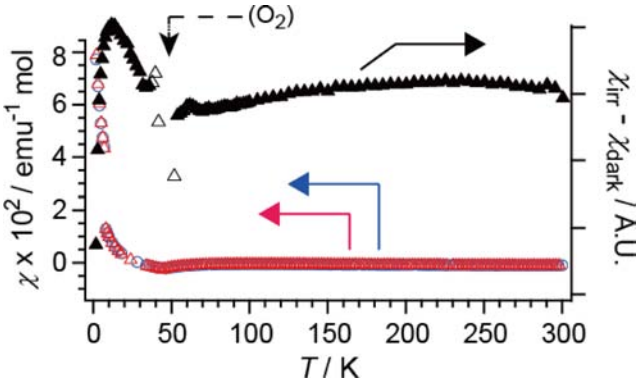

Figure 6. Magnetic susceptibility of BPY[Ni(dmit)$_2$]$_2$ under the dark condition and under UV irradiation. Under dark, both data of heating (red triangles) and cooling (blue circles) processes are shown, and core diamagnetism is corrected. Under dark, a jump at ~5 K is not intrinsic; it is produced after some scattered data points are removed. Total susceptibility happened to be close to 0 around ~5 K, which made data scattering in an irreproducible way. Under UV irradiation, open triangles around 50 K indicate the noise due to oxygen.

The same material exhibits qualitatively different magnetic behavior under UV irradiation (Figure 6). The difference in the susceptibilities under the dark and irradiated conditions ($\Delta\chi \equiv \chi_{irr} - \chi_{dark}$) effectively manifests the temperature dependence of χ_{irr}, because χ_{dark} is temperature independent, except for $T \leq 15$ K (Curie tail due to oxygen and lattice defects). From ~50 to 300 K, $\Delta\chi$ is nearly temperature independent and exhibits only a slight broad maximum at ~200 K. This behavior can be interpreted as Pauli paramagnetism, with the strong correlation due to the small band widths of BPY[Ni(dmit)$_2$]$_2$. From ~50 to ~10 K, $\Delta\chi$ begins to increase with decreasing temperature. This observation indicates the existence of localized spins. For $T \leq 10$ K, a sharp decrease in $\Delta\chi$ is observed. Such low-temperature behavior ($T \leq 50$ K) suggests a strong antiferromagnetic interaction between the localized spins in photoexcited BPY[Ni(dmit)$_2$]$_2$. It should be noted here that the localized spins are only on photoexcited cation (BPY^{2+})*, and they cannot directly interact with each other because every (BPY^{2+})* is surrounded by photoexcited anion ([Ni(dmit)$_2$]$^-$)*. Accordingly, the strong antiferromagnetic interaction should involve the magnetic interaction between (BPY^{2+})* and ([Ni(dmit)$_2$]$^-$)*.

Electron Spin Resonance. The ESR spectra acquired in the dark are shown in Figure 7. This material exhibits a single peak at $g_1 = 2.036$ with a large line width (>20 mT at 293 K). Comparison with the ESR spectrum of [(n-C$_4$H$_9$)$_4$N][Ni(dmit)$_2$] at 293 K (g_{dmit} = 2.025 (∥), 2.015 (⊥)) and that of BPY·Br$_2$ under UV irradiation (g_{BPY} = 2.001 (293 K), 1.993 (153 K)) (Figure S3) indicates that the signal observed in the dark should be assigned to [Ni(dmit)$_2$]$^-$. At 293 K, the ESR signal is clear but too broad to discuss in a quantitative way (Figure S4). At 153 K, the line width becomes much smaller.

dx.doi.org/10.1021/ja306260b | J. Am. Chem. Soc. 2012, 134, 18656−18666

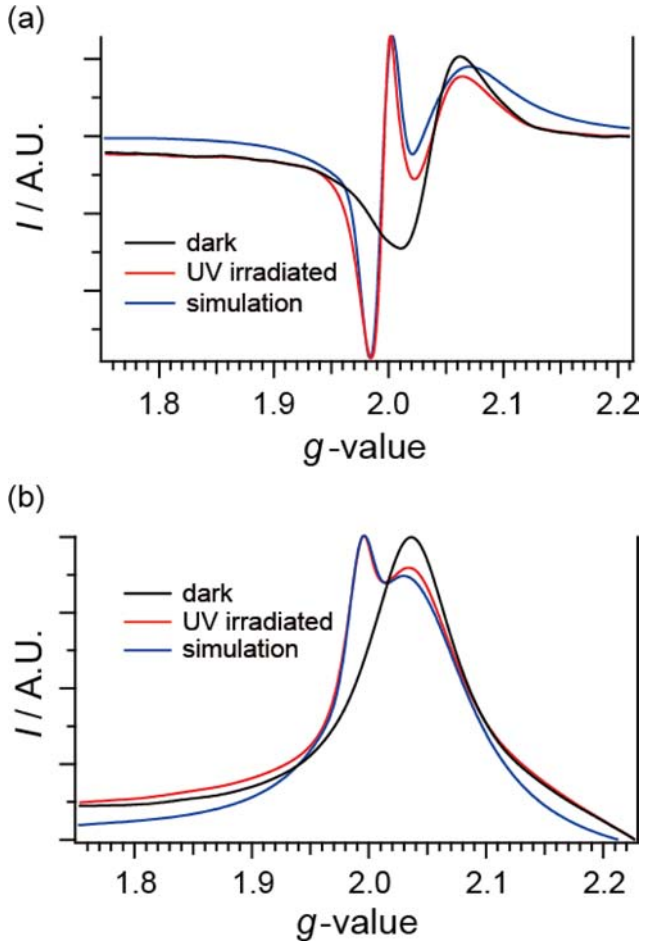

Figure 7. ESR spectra of the single crystal of BPY[Ni(dmit)$_2$]$_2$ measured under the dark condition and under UV (~250−450 nm; ~2 Wcm^{-2}) irradiation at 153 K, and simulated spectra using the parameters in Table S5: (a) as obtained and (b) first integral of (a). Magnetic field was applied perpendicular to [010].

Since the UV irradiation involves CT between BPY^{2+} and [Ni(dmit)$_2$]$^-$, the (BPY^{2+})* and ([Ni(dmit)$_2$]$^-$)* are tentatively called "CT-excited" states in order to distinguish them from photoexcited states without CT between the cation and the anion. Under UV (~250−450 nm) irradiation, an additional signal clearly appears in the ESR spectrum (Figure 7). The line shape indicates that the spectrum should contain two kinds of contributions from different types of spins. The g-values are g_1* = 2.034 and g_2* = 1.996. Judging from the g-values, the observed signals are assigned to the unpaired electrons on the CT-excited cation (BPY^{2+})* (g_2*) and the CT-excited anion ([Ni(dmit)$_2$]$^-$)* (g_1*). The relative line widths support this assignment, as delocalized (conduction) electrons generally exhibit larger ESR line widths than localized spins do. It should be noted here that the additional peak does not appear at any temperature without UV irradiation. In addition, the higher the temperature becomes, the less intense (BPY) or the broader (Ni(dmit)$_2$) the ESR signals become. This disagrees with the observations in Figures 7, S3b, and S4, and excludes the possibility that the additional peak originates substantially from heating effects.

The spectrum was simulated by assuming an electron spin (S = $^1/_2$) on the BPY and on the Ni(dmit)$_2$ species, and by considering the three-dimensional anisotropy of their g-values, line widths, and hyperfine interactions with ^{14}N (I = 1, natural abundance 99.635%) and ^{1}H (I = $^1/_2$, natural abundance 99.9844%) nuclei. The simulated spectrum reproduces the main feature of the observed spectrum well (Figure 7). The parameters obtained (Table S5) are consistent with those for other Ni(dmit)$_2$ radical anion complexes.[79] This material exhibits a stable and reversible response in the ESR under repetitive UV irradiation (Figure S5).

The amount of CT under UV irradiated condition can be roughly estimated from the change in ESR intensity, which indicates an ~10% decrease in charge on the Ni(dmit)$_2$ anions under UV irradiation ($\delta \approx 0.10$ in [Ni(dmit)$_2$]$^{(1-\delta)-}$). This value is consistent with the band calculation: $\delta \approx 0.25 \times 0.33 \approx 0.08$ by applying (the summation of) eq 1 to the bands located at ~2.75−5 eV (250−450 nm) above E_F. This is fairly good agreement, despite the rough estimation.

Mechanism and Possibility of PIPT in BPY[Ni(dmit)$_2$]$_2$. Here we will discuss some possible mechanism, which do not exclude other possibilities and should be elucidated by further studies. Some of the optical transitions in the UV region in BPY[Ni(dmit)$_2$]$_2$ are assigned to intermolecular LUMO→(-LUMO+n) ($n \geq 2$) transitions between Ni(dmit)$_2$ species. However, the (LUMO+2) and higher levels of Ni(dmit)$_2$ are practically localized levels in this material, unable to provide the high electrical conduction observed. Accordingly, UV irradiation does not appear to produce so evident a σ_{ph} in this material unless some active role of BPY is taken into consideration. The UV irradiation brings about the CT transitions between BPY^{2+} and [Ni(dmit)$_2$]$^-$ as well as between the [Ni(dmit)$_2$]$^-$ themselves (Figure 2). The latter CT transitions are also possible upon UV irradiation of other Ni(dmit)$_2$ complexes, which, however, hardly produces any σ_{ph} (Figure 5c). Therefore, the discussion thus far indicates a strong connection between a large σ_{ph} and cation−anion interactions, i.e., the importance of the CT transition between cation and anion. The CT transitions in this material have the character of a solid-state (reversible) photochemical redox reaction. The large sum of the oscillator strengths (~0.33) in the UV region suggests a large number of electrons transferred between BPY^{2+} and [Ni(dmit)$_2$]$^-$. This type of CT transition is essentially similar to the optical transitions between the valence and conduction bands in standard photoconduction, yet the number of electrons transferred is characteristically larger than any other type of optical transition. This can be considered to originate from the photoinduced redox activity of the bipyridyl derivatives, and might account for the larger photoconduction than other Ni(dmit)$_2$ complexes without such photoreactive cations.

Another possible mechanism could be PIPT. Qualitative changes in the physical properties under UV irradiation might be less obvious in BPY[Ni(dmit)$_2$]$_2$ than in usual thermodynamic transitions because of the limited volume fraction of the UV affected part of the sample (within a few μm from the surface). The extremely narrow band at E_F means that the slightest change in band filling might result in a drastic change in the Fermi surface, which in turn may cause a structural/electronic transition. In this case, the transition is from an ionic to CT state, and the final (CT) state is characterized by partial charges on BPY$^{2(1-\delta)+}$ and [Ni(dmit)$_2$]$^{(1-\delta)-}$, intermediate between ionic and neutral states. This transformation is similar to the melting of charge ordering in (EDO-TTF)PF$_6$[2,3] and α-(ET)$_2$I$_3$,[4−10] and yet BPY[Ni(dmit)$_2$]$_2$ also exhibits a melting of the diamagnetic spin-ordering and produces new spins on

dx.doi.org/10.1021/ja306260b | J. Am. Chem. Soc. 2012, 134, 18656−18666

different molecules at the same time. Such a type of PIPT has not been reported. A detailed mechanism will be clarified by time-resolved experiments, and studies on related materials will reveal how universal PIPT occurs.

CONCLUSION

In the dark, BPY[Ni(dmit)$_2$]$_2$ is a diamagnetic semiconductor having narrow bands around the Fermi level. Although this material does not exhibit any phase transition in the dark, UV irradiation over a wide temperature range (200−300 K) makes it a magnetic conductor. This is different from the many cases of PIPT known to date, which require irradiation under particular thermodynamic conditions close to the original (i.e., dark state) phase transitions or at extremely low temperatures (<10 K). Analysis of ESR has established the existence of two different types of spins under UV irradiation: localized spins on (BPY^{2+})* and carriers on ([Ni(dmit)$_2$]$^-$)*. An interaction between carriers and localized spins is suggested by an extended Hückel calculation, UV−vis−NIR spectra, and magnetic susceptibility measurements under UV irradiation. This photoresponsive behavior might be understood as CT-based photoconduction or a (new) kind of PIPT. Whether the observed photoconduction is based on an unknown mechanism or not, this conduction change under UV irradiation involves ionic to charge-transfer state transformation. Further pursuit of related salts will reveal how general such valence transitions are and also clarify their relationship to PIPT.

EXPERIMENTAL SECTION

Materials and Methods. All chemicals were purchased as highest grade and used as received. [*n*-(C$_4$H$_9$)$_4$N][Ni(dmit)$_2$] was synthesized according to the literature.[80] BPY·Br$_2$ was prepared by refluxing 2,2′-bipyridyl (Wako Pure Chemical Industries, 2.00 g, 12.8 mmol) in 1,2-dibromoethane (Tokyo Chemical Industry, 75.0 g, 0.40 mol) for 3.5 h, followed by recrystallization from cold methanol/ether (Wako). Pale greenish gray fine crystals. Yield: 1.24 g (28%). Found (calcd): C, 39.53 (41.89); H, 4.10 (3.52); N, 7.71 (8.14). IR (KBr): ν/cm^{-1} 3058, 3043, 3004, 2950, 2865, 2051, 1612, 1496, 1461, 1419, 1373, 1319, 790, 713. UV−vis (CH$_3$CN): λ/nm (log ε) 218 (4.325), 250 (3.316), 258 (3.232), 308 (4.034), 318 sh (4.00). Single crystals of BPY[Ni(dmit)$_2$]$_2$ were obtained from a slow double decomposition of the saturated solutions. BPY·Br$_2$ (10 mg) and [*n*-(C$_4$H$_9$)$_4$N][Ni(dmit)$_2$] (10 mg) were respectively added in acetonitrile (Wako; 20 mL each) and were dissolved as much as possible using a supersonic wave machine. After filtration, one of the solutions was added to the other. The mixed solution stood in the dark for several days at RT to yield shiny black platelets or needles of ∼0.5−1 mm. Found (calcd): C, 26.16 (26.52); H, 2.00 (1.11); N, 2.62 (2.58). IR: 1339(C═C), 1060 (C═S), 507 (Ni−S) (for the IR spectra, see Figure S6). Single-crystal X-ray structural analysis was carried out with a Rigaku Saturn724 diffractometer using multilayer mirror monochromated Mo Kα radiation (λ = 0.7107 Å) at 120 ± 1 K. The details of the structural analysis are described in the Supporting Information along with the CIF file, which is also deposited to CCDC as file 884912, and can be obtained free of charge from The Cambridge Crystallographic Data Centre via www.ccdc.cam.ac.uk/data_request/cif. For the calculation of UV−vis−NIR spectra of the monoradical anion [Ni(dmit)$_2$]$^-$ using Gaussian09,[72,73] the time-dependent (TD) method was utilized to determine the energy levels of the lowest six excited states. The basis set was B3LYP/6-31+G(3d,3pd). The initial molecular geometry was imported from the CIF file obtained from the single-crystal X-ray structural analysis on BPY[Ni(dmit)$_2$]$_2$, and optimization of the molecular structure was not carried out prior to the calculation.

UV Irradiation. Different light sources with band-pass filters ($\Delta\lambda$ = 40−60 nm), Notch filters (UVA, UVB, vis for 300−400, 240−300 and 400−700 nm) and/or optical fibers were used to examine the photoconductivity; Hg/Xe lamp (SAN-EI Electric, SUPERCURE-203S; 200 W, 220−1100 nm), Xe lamp (Asahi Spectra, LAX-Cute; 100 W, 200−1100 nm), D$_2$/tungsten-halogen lamp (Hamamatsu Photonics K.K., L7893; 30 W (D$_2$) and 5 W (halogen), 200−1100 nm, high-power tungsten-halogen lamp (Spectral Products, model ASBN-W100F-L; 100 W, 300−2600 nm), and laser (NEOARK; max. 20 mW with adjustable focus and intensity, 375 ± 5 nm). Actual light power of a particular wavelength was measured using a Si-diode power meter (OPHIR, NOVA). The details of the specifications of the light sources used in this work were described in our previous papers.[81,82]

Physical Property Measurements. Except for the magnetic susceptibility, all the single crystals were briefly checked by X-ray oscillation photographs to identify the crystal quality and the directions of the crystallographic axes. As for the magnetic susceptibility measurements, several of the single crystals were subjected to X-ray oscillation photographs to identify the crystal phase. Other details of electrical resistivity, magnetic susceptibility, and ESR measurements are described in Supporting Information.

ASSOCIATED CONTENT

Supporting Information

Physical properties under the dark condition, detailed procedures and results of X-ray structural analysis, spectroscopic data, and a comprehensive description of physical property measurements. This material is available free of charge via the Internet at http://pubs.acs.org.

AUTHOR INFORMATION

Corresponding Author

tnaito@ehime-u.ac.jp

Notes

The authors declare no competing financial interest.

ACKNOWLEDGMENTS

T.N. thanks R. Kato for discussion on the explanation of the observed physical properties. This study is partially supported by Grants-in-Aid for Scientific Research, Scientific Research(C) (No. 23540432) from Japan Society for the Promotion of Science (JSPS).

REFERENCES

(1) *Molecular electronic and related materials—control and probe with light*; Naito, T., Ed.; Research Signpost: Trivandrum, India, 2010; p 1.
(2) Chollet, M.; Guerin, L.; Uchida, N.; Fukaya, S.; Shimoda, H.; Ishikawa, T.; Matsuda, K.; Hasegawa, T.; Ota, A.; Yamochi, H.; Saito, G.; Tazaki, R.; Adachi, S.; Koshihara, S. *Science* **2005**, *307*, 86−89.
(3) Zhu, Y.; Itatani, J.; Rini, M.; Cavalleri, A.; Onda, K.; Ishikawa, T.; Ogihara, S.; Koshihara, S.; Shao, X.; Yamochi, H.; Saito, G.; Schoenlein, R. W. *Conference on Lasers and Electro-Optics/Quantum Electronics and Laser Science Conference and Photonic Applications Systems Technologies*; San Jose, CA, May 4, 2008; paper QThC6.
(4) Tajima, N.; Fujisawa, J.; Naka, N.; Ishihara, T.; Kato, R.; Nishio, Y.; Kajita, K. *J. Phys. Soc. Jpn.* **2005**, *74*, 511−514.
(5) Tajima, N.; Fujisawa, J.; Kato, R. Photo-switching between charge-ordered insulator and metal phases in an organic conductor α-(BEDT-TTF)$_2$I$_3$. In *Molecular electronic and related materials—control and probe with light*; Naito, T., Ed.; Research Signpost: Trivandrum, India, 2010; pp 155−165.
(6) Iimori, T.; Naito, T.; Ohta, N. *J. Am. Chem. Soc.* **2007**, *129*, 3486−3487.
(7) Iimori, T.; Ohta, N.; Naito, T. *Appl. Phys. Lett.* **2007**, *90*, 262103.
(8) Iimori, T.; Naito, T.; Ohta, N. Syneregy effects of photo-irradiation and applied voltage on electrical conductivity of α-(BEDT-TTF)$_2$I$_3$. In *Molecular electronic and related materials—control and probe with light*; Naito, T., Ed.; Research Signpost: Trivandrum, India, 2010; pp 167−184.

(9) Yamamoto, K.; Iwai, S.; Boyko, S.; Kashiwazaki, A.; Hiramatsu, F.; Okabe, C.; Nishi, N.; Yakushi, K. *J. Phys. Soc. Jpn.* **2008**, *77*, 074709.
(10) Yamamoto, K.; Yakushi, K. Second-harmonic generation study of ferroelectric organic conductors α-(BEDT-TTF)$_2$X (X = I_3, I_2Br). In *Molecular electronic and related materials—control and probe with light*; Naito, T., Ed.; Research Signpost: Trivandrum, India, 2010; pp 185−201.
(11) Tomić, S.; Jérome, D.; Bechgaard, K. *J. Phys. C: Solid State Phys.* **1984**, *17*, L655−L660.
(12) Gomes, H. L.; Stallinga, P.; Murgia, M.; Biscarini, F.; Muck, T.; Wagner, V.; Smits, E.; de Leeuw, D. M. *Proc. SPIE—Int. Soc. Opt. Eng.* **2005**, *5940*, 59400K/1−59400K/8.
(13) Niizeki, S.; Yoshikane, F.; Kohno, K.; Takahashi, K.; Mori, H.; Bando, Y.; Kawamoto, T.; Mori, T. *J. Phys. Soc. Jpn.* **2008**, *77*, 073710.
(14) Girlando, A.; Masino, M.; Painelli, A.; Drichko, N.; Dressel, M.; Brillante, A.; Della Valle, R. G.; Venuti, E. *Phys. Rev. B* **2008**, *78*, 045103.
(15) Girlando, A. *J. Phys. Chem. C* **2011**, *115*, 19371−19378.
(16) Girlando, A.; Masino, M.; Kaiser, S.; Sun, Y.; Drichko, N.; Dressel, M.; Mori, H. *Phys. Status Solidi B* **2012**, *249*, 953−956.
(17) Kumai, R.; Horiuchi, S.; Fujioka, J.; Tokura, Y. *J. Am. Chem. Soc.* **2012**, *134*, 1036−1046.
(18) Koshihara, S.; Takahashi, Y.; Sakai, H.; Tokura, Y.; Luty, T. *J. Phys. Chem. B* **1999**, *103*, 2592−2600.
(19) Okamoto, H.; Ishige, Y.; Tanaka, S.; Kishida, H.; Iwai, S.; Tokura, Y. *Phys. Rev. B* **2004**, *70*, 165202.
(20) Gütlich, P.; Hauser, A.; Spiering, H. *Angew. Chem., Int. Ed. Engl.* **1994**, *33*, 2024−2054.
(21) Decurtins, S.; Gütlich, P.; Köhler, C. P.; Spiering, H.; Hauser, A. *Chem. Phys. Lett.* **1984**, *105*, 1−4.
(22) Hayami, S.; Danjyobara, K.; Inoue, K.; Ogawa, Y.; Matsumoto, N.; Maeda, Y. *Adv. Mater.* **2004**, *16*, 869−872.
(23) Hayami, S.; Hiki, K.; Kawahara, T.; Maeda, Y.; Urakami, D.; Inoue, K.; Ohama, M.; Kawata, S.; Sato, O. *Chem.—Eur. J.* **2009**, *15*, 3497−3508.
(24) Ohkoshi, S.; Tsunobuchi, Y.; Matsuda, T.; Hashimoto, K.; Namai, A.; Hakoe, F.; Tokoro, H. *Nat. Chem.* **2010**, *2*, 539−545.
(25) Ozaki, N.; Tokoro, H.; Hamada, Y.; Namai, A.; Matsuda, T.; Kaneko, S.; Ohkoshi, S. *Adv. Funct. Mater.* **2012**, *22*, 2089−2093.
(26) Kato, R.; Kobayashi, H.; Kobayashi, A. *J. Am. Chem. Soc.* **1989**, *111*, 5224−5232.
(27) Hünig, S.; Erk, P. *Adv. Mater.* **1991**, *3*, 225−236.
(28) Hünig, S. *J. Mater. Chem.* **1995**, *5*, 1469−1479.
(29) Kato, R. *Bull. Chem. Soc. Jpn.* **2000**, *73*, 515−534.
(30) Hünig, S. *Chem. Rev.* **2004**, *104*, 5535−5563.
(31) Kanoda, K. *J. Phys. Soc. Jpn.* **2006**, *75*, 051007.
(32) Kobayashi, A.; Kato, R.; Kobayashi, H.; Mori, T.; Inokuchi, H. *Solid State Commun.* **1987**, *64*, 45−51.
(33) Mori, T.; Inokuchi, H.; Kobayashi, A.; Kato, R.; Kobayashi, H. *Phys. Rev. B: Cond. Matter Mater. Phys.* **1988**, *38*, 5913−5923.
(34) Kobayashi, H.; Miyamoto, A.; Kato, R.; Kobayashi, A.; Nishio, Y.; Kajita, K.; Sasaki, W. *Solid State Commun.* **1989**, *72*, 1−5.
(35) Miyamoto, A.; Kobayashi, H.; Kato, R.; Kobayashi, A.; Nishio, Y.; Kajita, K.; Sasaki, W. *Chem. Lett.* **1992**, *21*, 115−118.
(36) Nishio, Y.; Kajita, K.; Sasaki, W.; Kato, R.; Kobayashi, A.; Kobayashi, H. *Solid State Commun.* **1992**, *81*, 473−476.
(37) Kobayashi, H.; Miyamoto, A.; Kaot, R.; Sakai, F.; Kobayashi, A.; Yamakita, F.; Furukawa, Y.; Tasumi, M.; Watanabe, T. *Phys. Rev. B* **1993**, *47*, 3500−3510.
(38) Kobayashi, H.; Sawa, H.; Aonuma, S. *J. Am. Chem. Soc.* **1993**, *115*, 7870−7871.
(39) Tamura, M.; Sawa, H.; Aonuma, S.; Kato, R.; Kinoshita, M.; Kobayashi, H. *J. Phys. Soc. Jpn.* **1993**, *62*, 1470−1473.
(40) Sawa, H.; Tamura, M.; Aonuma, S.; Kato, R.; Kinoshita, M.; Kobayashi, H. *J. Phys. Soc. Jpn.* **1993**, *62*, 2224−2228.
(41) Aonuma, S.; Sawa, H.; Kato, R.; Kobayashi, H. *J. Chem. Soc., Perkin Trans. 2* **1995**, 1541−1549.
(42) Nishio, Y.; Tamura, M.; Kajita, K.; Aonuma, S.; Sawa, H.; Kato, R.; Kobayashi, H. *J. Phys. Soc. Jpn.* **2000**, *69*, 1414−1422.
(43) Tomić, S.; Jérome, D.; Aumüller, A.; Erk, P.; Hünig, S.; Von Schütz, J. U. *J. Phys. C: Solid State Phys.* **1988**, *21*, L203−L207.
(44) Tomić, S.; Jérome, D.; Aumüller, A.; Erk, P.; Hünig, S.; Von Schütz, J. U. *Europhys. Lett.* **1988**, *5*, 553−558.
(45) Kobayashi, H.; Tomita, H.; Naito, T.; Kobayashi, A.; Sakai, F.; Watanabe, T.; Cassoux, P. *J. Am. Chem. Soc.* **1996**, *118*, 368−377.
(46) Kobayashi, H.; Kobayashi, A.; Cassoux, P. *Chem. Soc. Rev.* **2000**, *29*, 325−333.
(47) Kobayashi, H.; Cui, H.-B.; Kobayashi, A. *Chem. Rev.* **2004**, *104*, 5265−5288.
(48) Ojima, E.; Fujiwara, H.; Kato, K.; Kobayashi, H.; Tanaka, H.; Kobayashi, A.; Tokumoto, M.; Cassoux, P. *J. Am. Chem. Soc.* **1999**, *121*, 5581−5582.
(49) Otsuka, T.; Kobayashi, A.; Miyamoto, Y.; Kiuchi, J.; Wada, N.; Ojima, E.; Fujiwara, H.; Kobayashi, H. *Chem. Lett.* **2000**, *29*, 732−733.
(50) Fujiwara, H.; Kobayashi, H. *Bull. Chem. Soc. Jpn.* **2005**, *78*, 1181−1196.
(51) Uji, S.; Shinagawa, H.; Terashima, T.; Yakabe, T.; Terai, Y.; Tokumoto, M.; Kobayashi, A.; Tanaka, H.; Kobayashi, H. *Nature* **2001**, *410*, 908−910.
(52) Matsuda, M.; Naito, T.; Inabe, T.; Hanasaki, N.; Tajima, H.; Otsuka, T.; Awaga, K.; Narymbetov, B.; Kobayashi, H. *J. Mater. Chem.* **2000**, *10*, 631−636.
(53) Hanasaki, N.; Tajima, H.; Matsuda, M.; Naito, T.; Inabe, T. *Phys. Rev. B* **2000**, *62*, 5839−5842.
(54) Hanasaki, N.; Matsuda, M.; Tajima, H.; Naito, T.; Inabe, T. *J. Phys. Soc. Jpn.* **2003**, *72*, 3226−3230.
(55) Inabe, T.; Tajima, H. *Chem. Rev.* **2004**, *104*, 5503−5533.
(56) Hanasaki, N.; Matsuda, M.; Tajima, H.; Ohmichi, E.; Osada, T.; Naito, T.; Inabe, T. *J. Phys. Soc. Jpn.* **2006**, *75*, 033703.
(57) Ishikawa, M.; Asari, T.; Matsuda, M.; Tajima, H.; Hanasaki, N.; Naito, T.; Inabe, T. *J. Mater. Chem.* **2010**, *20*, 4432−4438.
(58) Von Helmolt, R.; Wecker, J.; Holzapfel, B.; Schultz, L.; Samwer, K. *Phys. Rev. Lett.* **1993**, *71*, 2331−2333.
(59) Jin, S.; Tiefel, T. H.; McCormack, M.; Fastnacht, R. A.; Ramesh, R.; Chen, L. H. *Science* **1994**, *264*, 413−415.
(60) Wagner, P.; Gordon, I.; Trappeniers, L.; Vanacken, J.; Herlach, F.; Moshchalkov, V. V.; Bruynseraede, Y. *Phys. Rev. Lett.* **1998**, *81*, 3980−3983.
(61) Kubo, K.; Miyasaka, H.; Yamashita, M. *Physica B* **2010**, *405*, S313−S316.
(62) Hiraga, H.; Miyasaka, H.; Clérac, R.; Fourmigé, M.; Yamashita, M. *Inorg. Chem.* **2009**, *48*, 2887−2898.
(63) Hiraga, H.; Miyasaka, H.; Takaishi, S.; Kajiwara, T.; Yamashita, M. *Inorg. Chim. Acta* **2008**, *361*, 3863−3872.
(64) Imai, H.; Otsuka, T.; Naito, T.; Awaga, K.; Inabe, T. *J. Am. Chem. Soc.* **1999**, *121*, 8098−8103.
(65) Henrich, J. D.; Zhang, H.; Dutta, P. K.; Kohler, B. *J. Phys. Chem. B* **2010**, *114*, 14679−14688.
(66) Zhang, H.; Rajesh, C. S.; Dutta, P. K. *J. Phys. Chem. C* **2009**, *113*, 4623−4633.
(67) Kim, Y.; Das, A.; Zhang, H.; Dutta, P. K. *J. Phys. Chem. B* **2005**, *109*, 6929−6932.
(68) Lindqvist, O.; Andersen, J.; Sieler, J.; Steimecke, G.; Hoyer, E. *Acta Chim. Scand. Ser. A* **1982**, *36*, 855−856.
(69) Elmali, A.; Elerman, Y. *Anal. Sci.* **2002**, *18*, 855−856.
(70) Brownless, N. J.; Edwards, D. A.; Mahon, M. F. *Inorg. Chim. Acta* **1999**, *287*, 89−94.
(71) Ryan, T. M.; Day, R. J.; Cooks, R. G. *Anal. Chem.* **1980**, *52*, 2054−2057.
(72) Frisch, M. J.; Trucks, G. W.; Schlegel, H. B.; Scuseria, G. E.; Robb, M. A.; Cheeseman, J. R.; Scalmani, G.; Barone, V.; Mennucci, B.; Petersson, G. A.; Nakatsuji, H.; Caricato, M.; Li, X.; Hratchian, H. P.; Izmaylov, A. F.; Bloino, J.; Zheng, G.; Sonnenberg, J. L.; Hada, M.; Ehara, M.; Toyota, K.; Fukuda, R.; Hasegawa, J.; Ishida, M.; Nakajima, T.; Honda, Y.; Kitao, O.; Nakai, H.; Vreven, T.; Montgomery, Jr., J. A.; Peralta, J. E.; Ogliaro, F.; Bearpark, M.; Heyd, J. J.; Brothers, E.; Kudin, K. N.; Staroverov, V. N.; Kobayashi, R.; Normand, J.; Raghavachari, K.; Rendell, A.; Burant, J. C.; Iyengar, S. S.; Tomasi, J.; Cossi, M.; Rega,

N.; Millam, J. M.; Klene, M.; Knox, J. E.; Cross, J. B.; Bakken, V.; Adamo, C.; Jaramillo, J.; Gomperts, R.; Stratmann, R. E.; Yazyev, O.; Austin, A. J.; Cammi, R.; Pomelli, C.; Ochterski, J. W.; Martin, R. L.; Morokuma, K.; Zakrzewski, V. G.; Voth, G. A.; Salvador, P.; Dannenberg, J. J.; Dapprich, S.; Daniels, A. D.; Farkas, O.; Foresman, J. B.; Ortiz, J. V.; Cioslowski, J.; Fox, D. J. *Gaussian 09*, Revision C.01; Gaussian, Inc.: Wallingford, CT, 2009.

(73) Dennington, R.; Keith, T.; Millam, J. *GaussView*, Version 5; Semichem Inc.: Shawnee Mission, KS, 2009.

(74) For the difference between the calculation and experimental results, see footnote S3 in Supporting Information.

(75) Cassoux, P.; Valade, L.; Kobayashi, H.; Kobayashi, A.; Clark, R. A.; Underhill, A. E. *Coord. Chem. Rev.* **1991**, *110*, 115−160.

(76) Koshihara, S. *J. Lumin.* **2000**, *87*−*89*, 77−81.

(77) Yonemitsu, K. *J. Phys. Soc. Jpn.* **2004**, *73*, 2868−2878.

(78) Koshihara, S.; Adachi, S. *J. Phys. Soc. Jpn.* **2004**, *75*, 011005.

(79) Kirmse, R.; Stach, J.; Dietzsch, W.; Steimecke, G.; Hoyer, E. *Inorg. Chem.* **1980**, *19*, 2679−2685.

(80) Steimecke, G.; Sieler, H.-J.; Kirmse, R.; Hoyer, E. *Phosphorus Sulfur* **1979**, *7*, 49−55.

(81) Naito, T.; Sugawara, H.; Inabe, T.; Kitajima, Y.; Miyamoto, T.; Niimi, H.; Asakura, K. *Adv. Funct. Mater.* **2007**, *17*, 1663−1670.

(82) Naito, T.; Inabe, T.; Niimi, H.; Asakura, K. *Adv. Mater.* **2004**, *16*, 1786−1790.

(83) Hirose, T.; Imai, H.; Naito, T.; Inabe, T. *J. Solid State Chem.* **2002**, *168*, 535−546.